Journal of Natural Gas Science and Engineering xxx (2016) 1–11

Contents lists available at ScienceDirect

Journal of Natural Gas Science and Engineering

journal homepage: www.elsevier.com/locate/jngse

Rock typing of tight gas sands: A case study in Lance and Mesaverde formations from Jonah field

Elshan Aliyev [a, *], Milad Saidian [a], Manika Prasad [a], Branch Russell [b]

[a] Colorado School of Mines, USA
[b] Exaro Energy III LLC, USA

ARTICLE INFO

Article history:
Received 20 August 2015
Received in revised form
21 December 2015
Accepted 28 December 2015
Available online xxx

Keywords:
Tight gas sand
Jonah field
Rock typing
Pore size distribution
Permeability
Rock compressibility

ABSTRACT

The Jonah field is one of the biggest tight gas sand fields in the Green River basin. Production profiles from its deeper sections show high liquid hydrocarbons close to the Pinedale anticline, especially in Mesaverde and Lance formations. To assess the potential of condensate production, new approaches for rock classification are needed to differentiate between discontinuous sandstone layers and the interbedded siltstones. A gamma ray cut off of 75 API has been defined to distinguish between sandstone and siltstone in logs and core samples in Lance and Mesaverde formations. Significant variation of porosity and permeability occurs within the sandstone zones. This variation warrants new rock typing approaches. We present rock typing for tight sandstones and siltstones with an understanding of petrophysical properties such as pore structure, porosity, permeability, and cementation.

We studied 94 samples from the Mesaverde and Lance Formations with lithologies varying from clean sandstone to shale. X-ray diffraction (XRD) mineralogy, mercury injection capillary pressure (MICP), helium porosity and permeability were measured for all samples. NMR transverse relaxation times (T_2) at 2 MHz were also measured for 10 water saturated samples. Nitrogen adsorption was performed on 11 samples from Mesaverde formation to determine pore volume and pore size distribution.

MICP data are used to subdivide rocks into three groups based on pore throat size distribution: reservoir sandstones, non-reservoir sandstone and siltstone/mudstone. Dominant pore throat size for reservoir and non-reservoir sandstones are 400 and 100 nm, respectively. In order to apply pore throat size rock typing to downhole measurements, correlation between NMR pore size and MICP throat size is used. Pore size from NMR demonstrated equivalent behavior to pore throat size from MICP. The logarithmic mean values of T_2 transverse relaxation times for reservoir, non-reservoir sandstone and siltstone/mudstone are 22.2 ms, 3.4 ms and 0.29 ms, respectively. Clear separation of reservoir sandstone, non-reservoir sandstone and siltstone is also seen based on pressure dependency of ultrasonic compressional and shear velocities during initial pressure loading. Reservoir sandstone demonstrates the highest compressibility. In addition, siltstone and mudstone were separated based on log differential pore volume distribution from N_2 adsorption data.

Based on pore size distribution data, four main rock types are identified in Lance and Mesaverde formations in Jonah field. Rock typing based on gamma ray and porosity logs can be considered as rock classification of end members. To capture transitional behavior in between end members, pore size distribution is needed in logging application. Since NMR T_2 distribution show similar spectra to MICP throat size distribution, the rock typing technique can be applied using NMR log data. Separation of mudstone from siltstone can be used for identification of shale end points in log data.

1. Introduction

Jonah field is located in the Green River Basin (Fig. 1). It is bounded by two faults along the west and southeast and by a syncline that separates Jonah from the Pinedale anticline to the northeast. Sandstone, siltstone and mudstone were deposited in

* Corresponding author.
E-mail address: ealiyev@mines.edu (E. Aliyev).

http://dx.doi.org/10.1016/j.jngse.2015.12.045
1875-5100/

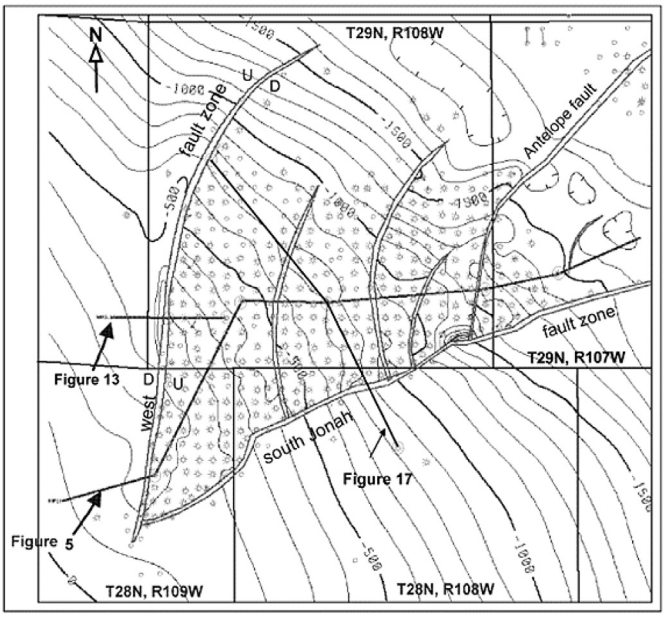

Fig. 1. Jonah field in Greater Green River basin. Field is located in Northern Greater Green River basin, and partially continues to the southeastern part of the Hoback basin (DuBois et al., 2004). (b) Structural map of Jonah field. The field is bounded by two faults from west and south and by Pinedale anticline on the north (Hanson et al., 2004).

fluvial channels during the Late Cretaceous (DuBois et al., 2004). The main productive formations are Lance and Mesaverde, which are also referred to as the Lance Pool (Fig. 2). Towards eastern margin of Jonah, the near top of the productive Lower Lance and Mesaverde formations are overlain by the so-called Dead Zone which is composed of impermeable claystone and probably represents lake deposits.

Reservoir development complexities in the Jonah field include discontinuous, thin, individual sandstone bodies with significant internal lithology variations as well as borehole enlargements due to unstable mudstone zones. Understanding rock properties of different formations can reduce inaccuracies in formation evaluation and improve future development of the Jonah field. Proper rock classification in tight gas sandstones requires understanding of the local mechanisms that control the physical properties of rocks such as deposition and diagenesis. These mechanisms in tight sandstones are mainly cementation and clay effects on pore geometry. As a result, porosity is locally reduced by cementation of quartz, chlorite, kaolinite, illite and sparse ferroan calcite which decrease pore throat size, clog pores and restrict fluid flow (DuBois et al., 2004).

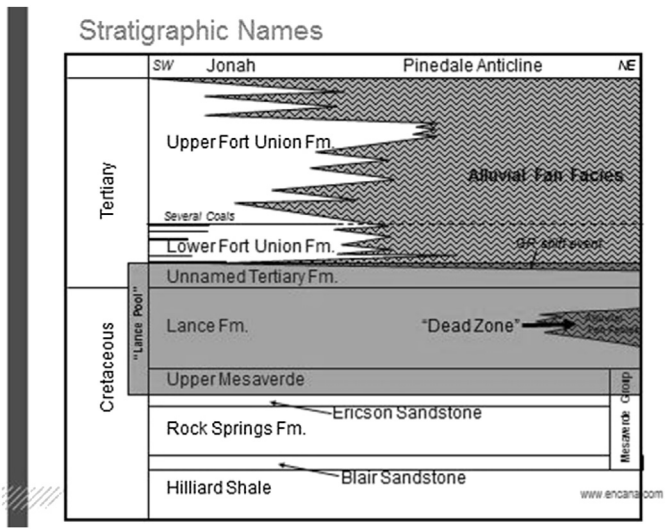

Fig. 2. Jonah Reservoirs. Lance and Mesaverde are the main productive formations and, are sealed by the so-called Tertiary formation "Dead Zone" from the top in eastern side of the field which is the main focus of the recent field development activities (Courtesy of Encana).

Formations in Jonah field are described as sandstone channels intercalated with siltstones and mudstones; the sandstones with porosity between 1 and 12% are considered main productive formations (Cluff and Cluff, 2004). Traditionally, 75 API units of gamma ray cut off were used to differentiate sandstone from siltstone and mudstone (DuBois et al., 2004). Siltstone and mudstone with GR > 75 API were disregarded in net pay calculations. Cluff and Cluff (2004) found that porosity less than 6% demonstrate poor rock quality, higher water saturation (>40%) and lower permeability (<5 μD). Therefore, insignificant fluid flow occurs from these types of rocks even after hydraulic fracturing.

Rock typing methods are broadly described in literature as the pore geometry, surface area, structure and mineralogy being staple controlling factors on permeability, porosity and capillary pressure (Archie, 1950; Pittman, 1992; Amaefule et al., 1993; Prasad, 2003; Rushing et al., 2008; Alam et al., 2011; Castillo et al., 2012). In this study we used hydraulic rock typing methods to identify different rock types in Lance and Mesaverde formations. We performed different rock typing methods to subdivide sandstone into different rock groups based on available core helium porosity and permeability data from Lance formation. We also utilized experimental methods such as MICP, NMR and nitrogen adsorption to further differentiate rock types based on pore size distribution, clay content, cementation and we evaluated acoustic velocities as additional information for rock typing.

2. Material and methods

We studied 94 samples from Lance and Mesaverde formations for rock typing study. We chose 14 core samples, representing different facies from Mesaverde formation, for further experimental study (experimental data for other 80 samples were provided by the vendors). The samples were predominantly quartz (up to 90 wt%) with moderate amounts of clay (up to 60 wt%, predominantly illite) and small amounts of carbonates (up to 17 wt%) (Fig. 3).

2.1. Helium injection

Helium porosity and permeability were measured with a CMS-300™ apparatus for 94 samples from Lance and Mesaverde formations. The system uses nitrogen gas to provide confining stress. Pore pressure was provided by helium gas which measured permeability and pore volume.

2.2. Mercury injection capillary pressure (MICP)

Capillary pressure measurements were performed on 30 samples from Lance and Mesaverde formation. After degassing intact rock chips at 200 °C for 12 h, mercury was injected into samples at pressure steps from 0 to 60,000 psi. The Washburn (1921) equation was used to convert pressure data to the throat size distribution. To consider rock compressibility effect at high pressure steps, a conformance correction was applied using Bailey method (Comisky et al., 2011). Total porosity was calculated from cumulative

Please cite this article in press as: Aliyev, E., et al., Rock typing of tight gas sands: A case study in Lance and Mesaverde formations from Jonah field, Journal of Natural Gas Science and Engineering (2016), http://dx.doi.org/10.1016/j.jngse.2015.12.045

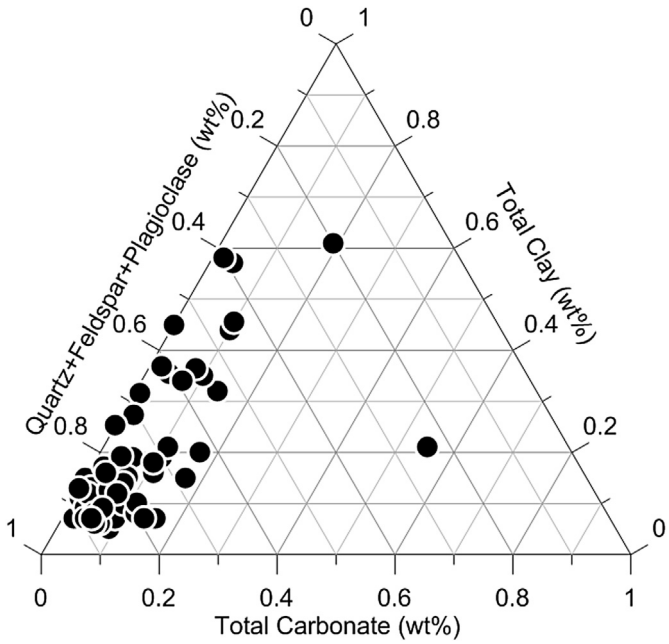

Fig. 3. Mineralogy of samples from Lance and Mesaverde formations from Jonah field. The samples were predominantly quartz (up to 90 wt%) with moderate amounts of clay (up to 60 wt% predominantly illite) and small amounts of carbonates (up to 17 wt %).

distribution of injected mercury volume. Theoretically, mercury can assess pores with throat diameter bigger than 3.6 nm. For data analysis, both gas–water and air–mercury systems were used. In case of gas–water, the capillary pressure data were converted to reservoir condition from laboratory mercury–air system.

2.3. Nuclear magnetic resonance (NMR)

A 2 MHZ Magritek™ NMR Rock Core Analyzer was utilized for transverse relaxation time (T_2) measurements. T_2 was measured for the 10 fully brine saturated samples using Carr–Purcell–Meiboom–Gill (CPMG) (Carr and Purcell, 1954; Meiboom and Gill, 1958) pulse sequence at ambient pressure and temperature conditions. In order to avoid clay swelling, distilled water was mixed with crushed clay-rich samples for 24 h to reach equilibration. Then the mixture was used to saturate samples under vacuum condition for two days. Samples were wrapped carefully with plastic to minimize the evaporation of the saturating fluid during the experiment. The NMR response was acquired with 100 μs echo spacing for all samples, inter experimental delay of 4000 ms and 1000 ms, number of echoes of 6000 and 1000 and minimum signal to noise ratio of 200 and 100, for high porosity (sandstone) and low porosity (siltstone) samples, respectively. An inverse Laplace transform (Butler et al., 1981; Dunn et al., 1994) was used to invert the raw echo train data to T_2 distribution.

2.4. Nitrogen adsorption

Nitrogen adsorption was performed on 11 samples from Mesaverde formation using a Micromeritics ASAP 2020™ instrument to determine pore volume and pore-size distribution. 1–3 g of sample was degassed for 24 h at 200 °C temperature in vacuum condition to remove water and moisture from the sample chips. Subsequently, the samples were dosed with nitrogen at sub-atmospheric pressures and subcritical temperature (at 77 K). Pore size distribution (PSD) was inverted using Barrett, Joyner and Halenda (BJH) technique (Barrett et al., 1951), which assumes pores as non-connected cylinders. Pore volume was calculated from adsorbed nitrogen amount in a pore size range of 1.7–193.5 nm, which is the measurable range of pores by nitrogen adsorption method. Micropore volume (pore size < 1.7 nm) was determined from t-plot technique using Harkins and Jura (1944) method.

2.5. Ultrasonic velocity

For this study 10 cores were used for ultrasonic velocity measurements under confining pressure condition with no pore pressure. Compressional (P) and two orthogonal shear (S1, S2) velocities were measured from the top sides of cylindrical cores at 1 MHz frequency up to 5000 psi confining pressure at 500 psi steps. Confining pressure was provided by hydraulic oil.

3. Rock typing with hydraulic units

In this section we show methodology and results for three rock typing techniques: flow zone indicator, effective specific surface and hydraulic rock typing. Porosity and permeability are correlated using pore geometry factors, effective specific surface area and pore throat radius.

3.1. Flow zone indicator (FZI)

Flow zone indicator correlates permeability with porosity considering pore geometry factors. Porosity is the volumetric property of rock and does not depend on pore structure. However, permeability depends on the shape, distribution and connectivity of the pores and surface area of the grains which are in contact with flowing fluid. To delineate permeability–porosity correlation, Amaefule et al. (1993) modified Kozeni–Carman equation as following:

$$FZI = \frac{RQI}{\varepsilon} \tag{1}$$

Where, $FZI = 1/\sqrt{F_s}\tau S_{V_{gr}}$ is flow zone indicator. It accounts for pore geometry and does not depend on permeability and porosity. $RQI = 0.0314\sqrt{k/\phi}$ is reservoir quality index. The factor 0.0314 accounts for permeability unit conversion from μm^2 to md. F_s is the pore shape factor, τ is tortuosity, $S_{V_{gr}}$ is the specific surface area per unit grain volume, k is permeability (μm^2) and ϕ is porosity in fraction, and $\varepsilon = \phi/(1-\phi)$ is Void ratio, which is the ratio of pore volume to solid volume.

Fig. 4a is a demonstration of rock classification based on porosity and permeability. Four rock types are identified with different FZI units. Rock quality increases with increasing FZI values. Low porosity and permeability rocks fall in rock type I which has the highest rock quality.

3.2. Effective specific surface (ESS)

Effective specific surface area method correlates permeability and porosity with S_g term which is specific surface area of grains exposed to fluid flow. Porous media in tight sandstones was subjected severe cementation (Vernik and Kachanov, 2010). Clay filling, quartz/clay overgrowth and carbonate cementation can disconnect pores and severely increase tortuosity. Due to complex pore structure, fluid flow can occur parallel or orthogonal to the direction of pressure drop (Alam et al., 2011). Mortensen et al. (1998) used the term active porosity to describe the main part of pore space contributing fluid flow. They considered pore space as orthogonal connected tubes. Fluid flow occurring in this type of

Please cite this article in press as: Aliyev, E., et al., Rock typing of tight gas sands: A case study in Lance and Mesaverde formations from Jonah field, Journal of Natural Gas Science and Engineering (2016), http://dx.doi.org/10.1016/j.jngse.2015.12.045

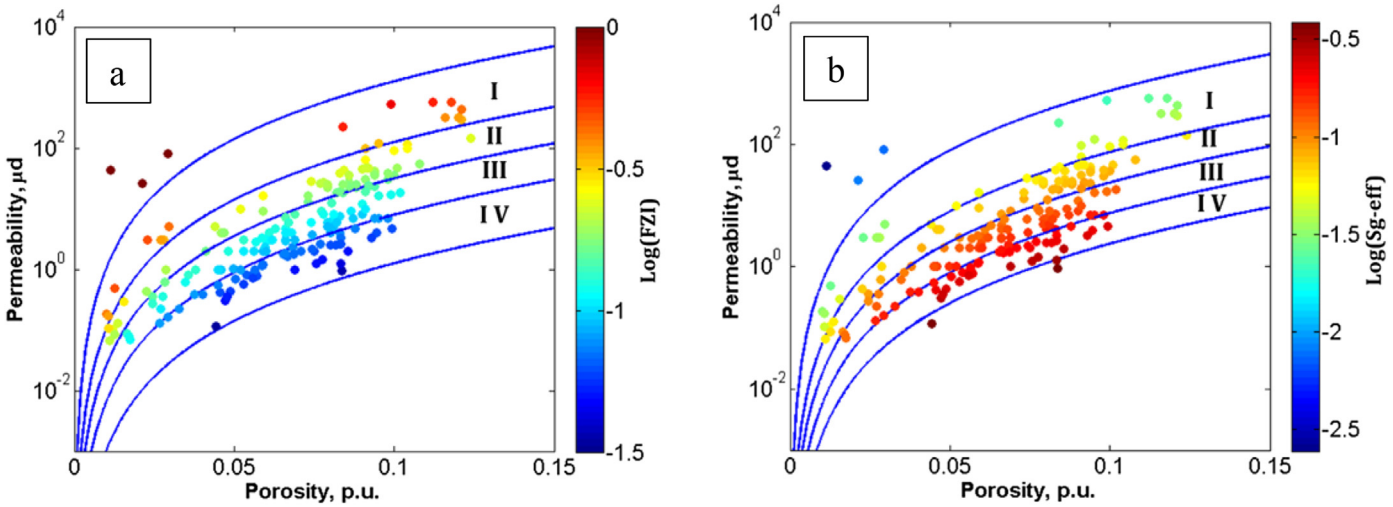

Fig. 4. Permeability and porosity classification of rocks from Lower Lance and Mesaverde formations of Jonah field (provided by Exaro Energy) based on log(FZI) = −1; −1.5; −1.1; −0.5; 0 (a) and log(S_{g-eff}) = −3.5; −2.5; −2; −1.5; −1 (b) values. Four rock types are identified when data is color-coded with FZI and S_{g-eff} values. In FZI method, rock quality is improving with increasing FZI values (a). However, in specific surface area method, rock quality improves with decreasing S_{g-eff} values (b).

pore space will be dependent on alignment of tubes with respect to the pressure drop. The active porosity replaced tortuosity and pore shape factor in Cozeny–Karman equation (Mortensen et al., 1998):

$$k = c(\phi)\frac{1}{S_{g-eff}^2}\frac{\phi^3}{(1-\phi)^2} \quad (2)$$

Effective specific surface S_{g-eff} in Equation (2) can be used as an independent parameter in the porosity–permeability correlation. S_{g-eff} can be measured with BET nitrogen adsorption technique. In the absence of laboratory data, S_{g-eff} can be calculated by solving Equation (2) for S_{g-eff}.

Fig. 4b demonstrates porosity–permeability correlation from two wells. Based on calculated S_{g-eff} values four rock types are identified. Rock quality increases with decreasing log(S_{g-eff}) values. The magnitude of S_{g-eff} is directly proportional to the clay content. Higher clay content is associated with poor connectivity of the pores, hence with lower permeability. In addition, clay fills pore space and decreases effective porosity. Therefore, there is an inverse relationship between S_{g-eff} and rock quality. Similar to FZI method (Fig. 4a), low porosity and permeability samples fall in rock type I which has the highest rock quality.

3.3. Hydraulic rock typing (HRT)

Hydraulic rock typing characterizes rocks based on different flow properties (Pittman, 1992). Differences in rock qualities are classified based on permeability. Finding the main pore throat radius which dominates fluid flow is the key in hydraulic rock typing. Thomeer (1960) suggested a methodology to identify the dominant pore throat radius using MICP data. Using this method, we found that the main throat radius corresponds to 35th percentile of injected mercury saturation for Lance and Mesaverde formations. Pittman (1992) derived a set of empirical equations, correlating the main pore throat radius, porosity and permeability at different percentiles of mercury saturation. Using the apex point of mercury saturations (35% percentile) the following equation is used to model permeability:

$$\log(k) = \frac{1}{0.565}(0.523\log(\phi) - \log(r_{35}) - 0.255) \quad (3)$$

Where, r_{35} (µm) is a radius relevant to the 35th percentile, k (md) is the Klinkenberg-corrected permeability and ϕ (%) is the porosity.

Helium porosity measured at 4000 psi differential pressure condition and four pore throat radii (r_{35}) were used as an input into the Equation (3) to subdivide rocks into different rock types. Four rock types based on permeability behavior from two wells can be seen in Fig. 5. The quality of rocks decreases from first to fourth type. The main rock types are HRT1, HRT2 and partially HRT3 (section with the porosity values > 6%). The fourth group mainly exhibits permeability <1 µd, porosity <6%, and bounded with the permeability model corresponding to R = 0.1 µm pore throat radius. These types of sandstones are considered non-reservoir rocks due to low permeability and tendency for high water saturation contents. The first and second types of rocks are reservoir sandstones.

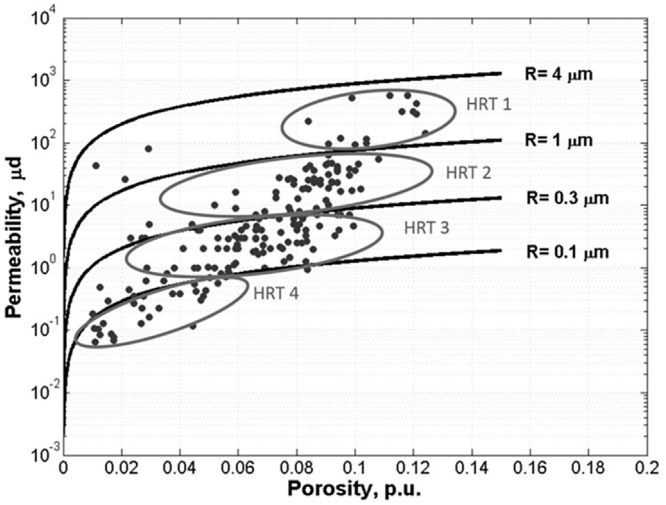

Fig. 5. Permeability classification of rocks using Pittman (1992) 35th percentile method for Lower Lance and Mesaverde formations. Four rock types are identified based on permeability behavior. The quality of rocks decreases from first to fourth type. Helium porosity and permeability were provided by Exaro Energy.

Please cite this article in press as: Aliyev, E., et al., Rock typing of tight gas sands: A case study in Lance and Mesaverde formations from Jonah field, Journal of Natural Gas Science and Engineering (2016), http://dx.doi.org/10.1016/j.jngse.2015.12.045

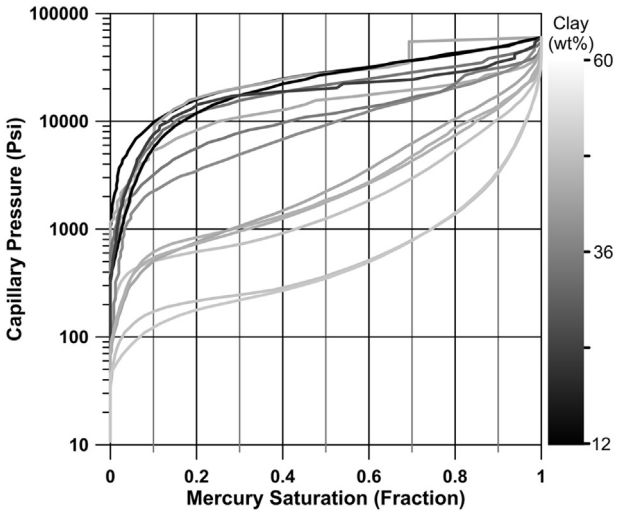

Fig. 6. MICP curves for mercury–air system, color coded with clay content. The capillary pressure is directly proportional to the clay content of the samples. High capillary pressure in some low clay samples is probably due to the carbonate cementation. In mercury–air system, capillary entry pressure starts from approximately 40–50 psi for the low clay (<15 wt%) samples and can increase up to 500 psi for high clay samples (>30 wt%).

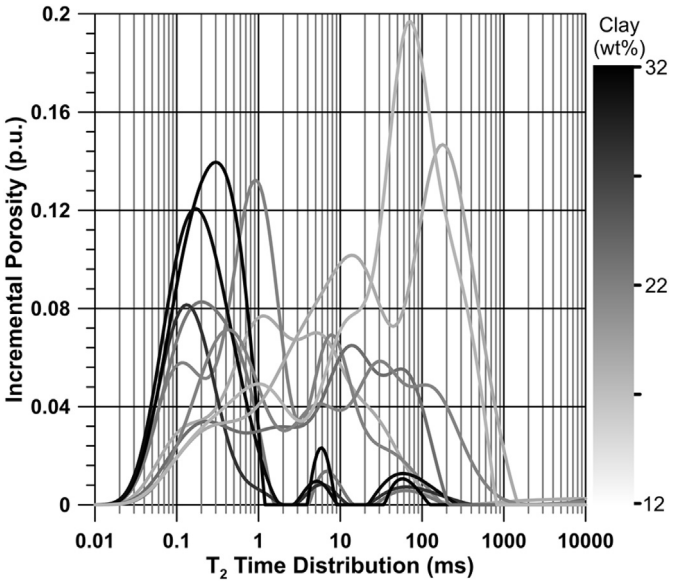

Fig. 8. T_2 relaxation time distribution results for 10 samples, color coded with clay content. High clay (>30 wt%) samples show faster relaxation times which represent smaller pore size ranges. Moderate clay (15–30 wt%) samples show a broad T_2 distribution which demonstrates presence of a wide range of pore sizes. The dominant T_2 time varies from 0.2 to 200 ms for high and low clay samples, respectively.

Permeability is varying from 1 to 100 μd for the second type and from 100 to 500 μd for the first type, respectively. Porosity variation is in the range of 6–12%. At porosity value of approximately 10%, the difference in permeability values between first and second rock type is one order of magnitude. Considering 0–12% as a reliable porosity range for sandstone formation, possible difference in the porosities for the two groups is smaller than permeability difference. Permeability depends on main pore throat size, rather than total porosity as dictated by HRT technique. Therefore, despite of slight variation in porosity, formation can be classified due to permeability behavior.

Note that, in comparison with the ESS and FZI methods, in HRT method, the low quality samples (low porosity and low permeability) belong to third and fourth rock types.

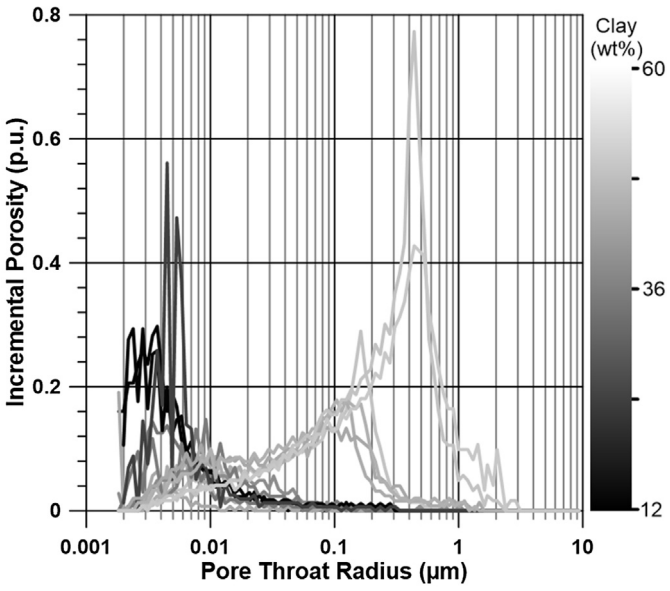

Fig. 7. Throat size distribution (TSD) for mercury–air system, color coded with clay content. High clay samples show smaller TSD. Note that the TSDs of high clay samples are not complete (black and dark grey curves around 0.002 μm). In other words, the mercury injection method does not describe the full spectra of TSDs. This suggests that there are pores with throat radius smaller than 1.8 nm which are not assessed by the mercury due to the limitation of this technique. The dominant throat size varies from 0.002 to 0.4 μm.

4. Experimental study

4.1. MICP

Figs. 6 and 8 show MICP curves and throat size distribution (TSD) for mercury–air system, color coded with clay content. In mercury–air system, capillary entry pressure starts from approximately 40–50 psi for the low clay (<15 wt%) samples and can increase up to 500 psi for high clay samples (>30 wt%) (Fig. 6). The capillary pressure is directly proportional to the clay content of the samples (High capillary pressure in some low clay samples is probably due to the carbonate cementation) (Fig. 6). High clay (>30 wt%) samples show higher pressure within the entire saturation interval (Fig. 6) as well as smaller TSD (Fig. 7). Incomplete throat size distribution at lower limit of the MICP technique (throat radius of 1.8 nm) for high clay (>30 wt%) samples suggests that suggests that there are pores with throat radius smaller than 1.8 nm that are not assessed by the mercury. This limitation is confirmed by underestimation of porosity measured by mercury intrusion in comparison with other techniques such as nitrogen adsorption and NMR (not shown here, for more information see Saidian et al., 2014). The dominant throat size varies from 0.002 to 0.4 μm (Fig. 7) for high and low clay samples, respectively.

4.2. NMR

Fig. 8 shows T_2 relaxation time distribution results for 10 samples, color coded with clay content. High clay (>30 wt%) samples show faster relaxation times which represent smaller pore size ranges. Moderate clay (15–30 wt%) samples show a broad T_2 distribution which demonstrates presence of a wide range of pore

Please cite this article in press as: Aliyev, E., et al., Rock typing of tight gas sands: A case study in Lance and Mesaverde formations from Jonah field, Journal of Natural Gas Science and Engineering (2016), http://dx.doi.org/10.1016/j.jngse.2015.12.045

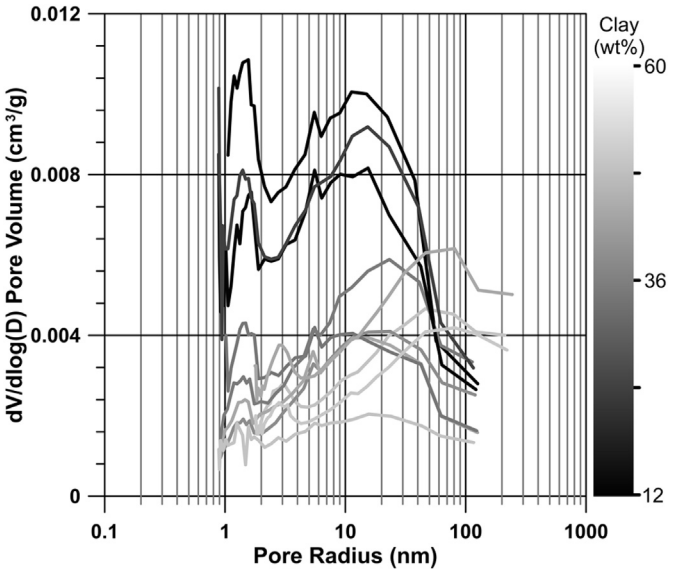

Fig. 9. The PSD of the samples measured by nitrogen adsorption technique. Due to limitations of this technique the PSD does not represent the whole pore spectra for low clay (<15 wt%) samples. The PSD amplitude and consequently the pore volume increase with increasing the clay content. This increase in amplitude is due to the abundance of small pores (1.7–200 nm) in samples with higher clays. Moderate and high clay (>15 wt%) samples show bimodal distribution. Shapes of the distributions suggest that there is a third mode that was not captured due to technique limitation (minimum pore diameter of 1.7 nm).

sizes. The dominant T_2 time varies from 0.2 to 200 ms for high and low clay samples, respectively.

4.3. Nitrogen adsorption

Fig. 9 shows the PSD of the samples measured by nitrogen adsorption technique. Due to limitations of this technique the PSD does not represent the whole pore spectra for low clay (<15 wt%) samples (for more information see Saidian et al., 2014). The PSD amplitude and consequently the pore volume increase with increasing the clay content. This increase in amplitude is due to the abundance of small pores (1.7–200 nm) in samples with higher clays. Moderate and high clay (>15 wt%) samples show bimodal distribution. Shapes of the distributions suggest that there is a third mode that was not captured due to technique limitation (minimum pore diameter of 1.7 nm). The amplitude of the third mode increases with increasing clay content which confirms the observation.

5. Discussion

We categorized samples with variable clay and carbonate content using different rock typing techniques and experiments. Different petrophysical properties of samples such as porosity, permeability, surface area, pore throat size distribution and NMR response were used to identify rock types in Mesaverde and Lance formation in Jonah field. In this section, first we compare different rock typing techniques and discuss their advantages and disadvantages. Then we use a combination of various experimental data to improve the rock typing honoring the mineralogical and textural variations of the samples.

5.1. Comparison of rock typing techniques

For porosity and permeability correlations, FZI and ESS methods use the pore geometry and effective specific surface area as a quality factor, respectively. These methods can be successfully applied to rock typing if quality factors are measured independently. In the absence of the laboratory data, both methods calculate the pore geometry and effective specific surface area using porosity and permeability. In this case, porosity and permeability will have equal weights in the calculation of log(FZI) and log(S_{g-eff}). As a result, low porosity and permeability rocks can give the same values of hydraulic units (log(FZI) and log(S_{g-eff})) as high porosity and permeability rocks (Fig. 4). Therefore, certain rock type possibly encompasses the entire range of porosity and permeability, which is not reliable.

Despite other rock typing techniques, in HRT classification low porosity and permeability rocks fall in poor quality rock types (Fig. 5). HRT correlates permeability with porosity based on dominant pore throat size, which is independently measured from capillary pressure data. In comparison with permeability, porosity is less sensitive to the pore throat size change. Therefore, HRT method can be considered as permeability classification of rocks (Fig. 5). Different permeability behavior for the first and second type of rocks in HRT classification demonstrated the importance of pore geometry in fluid flow properties.

5.2. Rock typing using experimental data

According to Rose and Bruce (1949), the shape of the capillary pressure curves is the primary indication of pore geometry. High capillary pressure shows the existence of small pore throats. Mercury is the non-wetting phase; hence high injection pressure is required for mercury to enter into the small pores. Fig. 6 shows capillary pressure response of air–mercury system. Three types of pressure behaviors can be detected from the shapes of the curves for 14 samples from Mesaverde formation. To represent reservoir condition, the same data is converted to gas–water system in Fig. 10. Black colored curves are siltstone and mudstone according to gamma ray classification (GR > 75 API), and exhibit highest

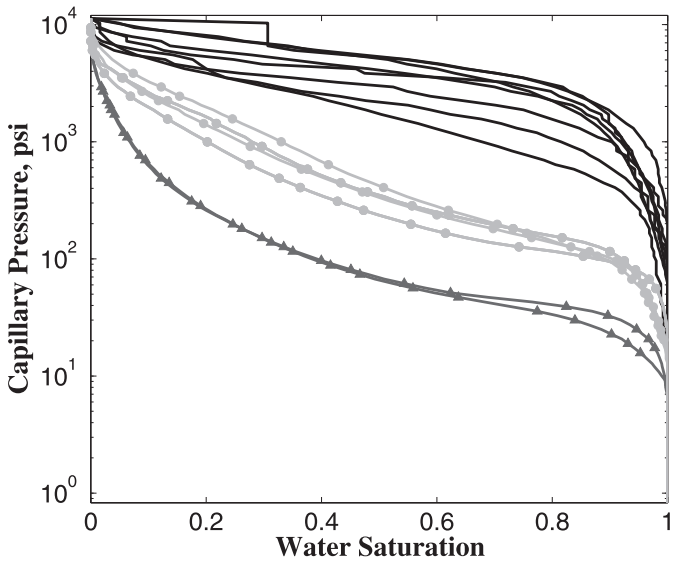

Fig. 10. Capillary pressure response of gas–water derived from air–mercury system. Three types of pressure behavior can be detected. Black colored curves are siltstone and mudstone according to gamma ray classification (GR > 75 API), and exhibit highest capillary pressure. Dark grey triangles and light grey circles are sandstones (GR < 75 API). Sandstones with light grey circles have mercury porosity values less than 6%. Good quality sandstone (dark grey triangles) possesses porosity value around 10%, which is the target formation for production.

Please cite this article in press as: Aliyev, E., et al., Rock typing of tight gas sands: A case study in Lance and Mesaverde formations from Jonah field, Journal of Natural Gas Science and Engineering (2016), http://dx.doi.org/10.1016/j.jngse.2015.12.045

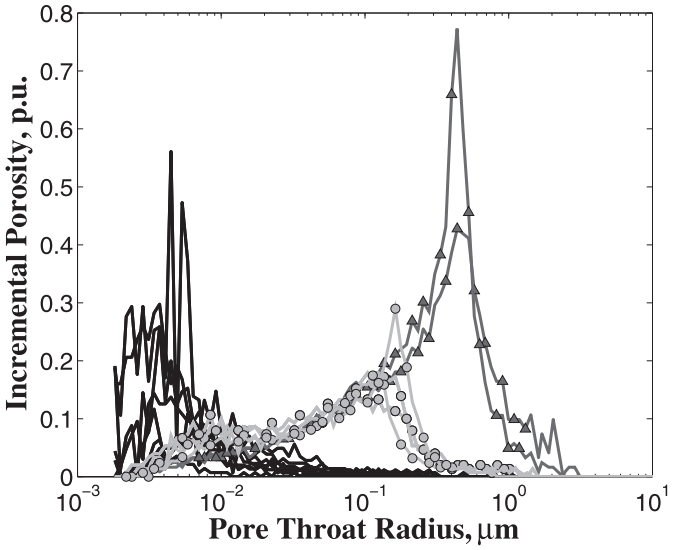

Fig. 11. Pore throat size distribution for three types of rocks: reservoir sandstone (dark grey triangles); non-reservoir sandstone (light grey circles); mudstone–siltstone (black colored curves). PSD for siltstone and mudstone falls in a range of 3.6–10 nm. In this range of PSD, productivity of the formations will be very low. Peak in PSD for good quality sandstone (dark grey triangles) occurs at 300–600 nm. Sandstones with porosity values less than 6% demonstrate wide range of PSD.

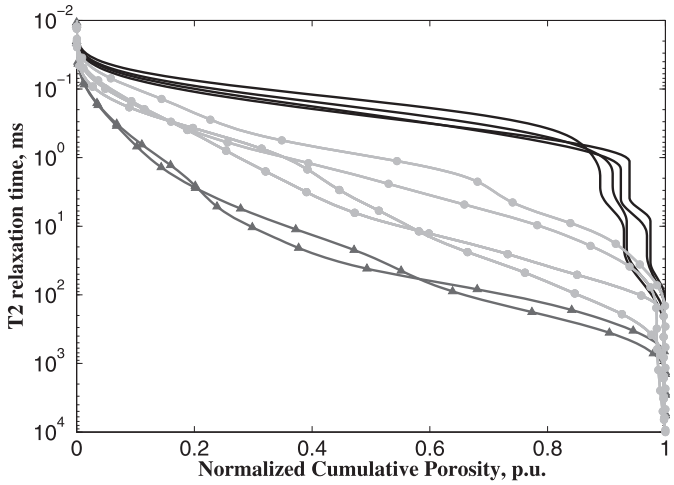

Fig. 12. NMR cumulative porosity for different rock types: reservoir sandstone (dark grey triangles); non-reservoir sandstone (light grey circles); mudstone–siltstone (black colored curves). The shape of the cumulative porosity from NMR exhibits equivalent behavior to capillary pressure curves from MICP. Siltstone demonstrates the shortest value of relaxation time, while non-reservoir and reservoir sandstones have the intermediate and the longest values, respectively.

capillary pressure. Dark grey triangles and light grey circles are sandstones (GR < 75 API). Sandstone group demonstrates two distinct rock types. Sandstones with light grey circles have the mercury porosity values less than 6%, hence is less important as the reservoir rock (intermediate capillary pressure system: non-reservoir sandstone). Good quality sandstone (dark grey triangles) has porosity value of approximately 10%, which is the target formation for production (low capillary pressure system: reservoir sandstone). In this classification, all types of rocks show good correlation between capillary pressure and porosity. Increase in capillary pressure is associated with decrement in porosity.

The difference in depth interval for reservoir and non-reservoir sandstone is very low (less than 8 ft). As the true vertical depth for core samples is more than 12,000 ft, drastic changes in physical properties are likely due to diagenesis rather than depositional compaction. The only visible difference between reservoir and non-reservoir sandstone is the presence of carbonates in non-reservoir rocks. In tight sandstone, carbonate cement can fill pores in between grains (Rushing et al., 2008).

To show the effect of pore geometry on rock classification, TSD for end members of each type of rock is derived from capillary pressure data (Fig. 11). Color-coding is remained same with capillary pressure data. TSD for siltstone and mudstone falls in a range of 3.6–10 nm (non-productive zone). Peak in TSD for good quality sandstone (dark grey triangles) occurs at 300–600 nm. Sandstones with porosity values less than 6% demonstrate wide range of TSD. More samples are required to provide more robust TSD cut off values for rock typing classification. Dominant pore size derived from HRT method is a better permeability indicator, rather than pore size range.

Rock classification is made based on MICP calculated pore throat distribution. Downhole measurements of TSD are impossible; therefore, this classification method cannot be applied to log data directly. NMR logging is the only tool that provides a representation of PSD of the rock at downhole condition. Rock classification based on PSD from NMR data can be used as an alternative for MICP for downhole applications.

The shape of the T_2 relaxation as a function of normalized cumulative porosity from NMR (Fig. 12) exhibits equivalent behavior to capillary pressure curves from MICP (Fig. 10). In Fig. 12, normalized cumulative porosity is equivalent to saturation, and T_2 relaxation times are inversely proportional to the pore size or capillary pressure. Siltstone demonstrates the shortest relaxation time, while non-reservoir and reservoir sandstones have the intermediate and the longest relaxation times, respectively. T_2 distributions are plotted in Fig. 13. Siltstone (black colored curves) and reservoir sandstone (dark grey triangles) show distinct groups. Higher clay content, consequently smaller pores and higher surface area of siltstones shifted the peak to the lower T_2 values. On the

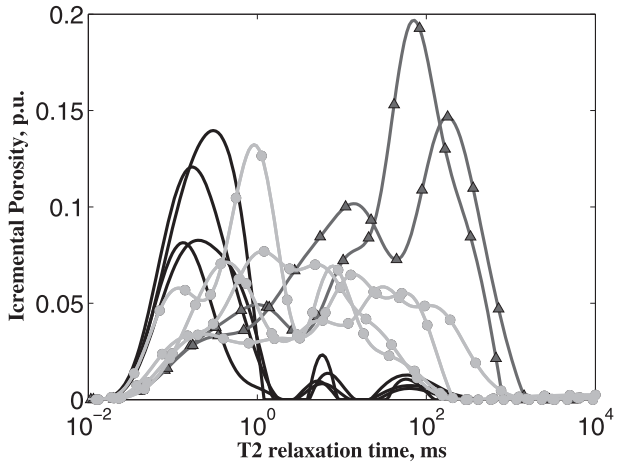

Fig. 13. T_2 distribution of incremental porosity: reservoir sandstone (dark grey triangles); non-reservoir sandstone (light grey circles); mudstone–siltstone (black colored curves). Siltstone and reservoir sandstone show clear separation of groups. Higher clay content, hence smaller pores of siltstones shifted the peak to the lower T_2 values. The presence of relatively bigger pores in reservoir sandstone group is associated with the longer relaxation time. Effect of cementation on pore and throat sizes in non-reservoir sandstone led to the wide range of T_2 without separation of dominant pore size response. The logarithmic mean of T_2 for each group can be averaged for NMR log interpretation purposes, which are 22.2 ms, 3.4 ms and 0.29 ms for reservoir, non-reservoir sandstones and siltstone, respectively.

Please cite this article in press as: Aliyev, E., et al., Rock typing of tight gas sands: A case study in Lance and Mesaverde formations from Jonah field, Journal of Natural Gas Science and Engineering (2016), http://dx.doi.org/10.1016/j.jngse.2015.12.045

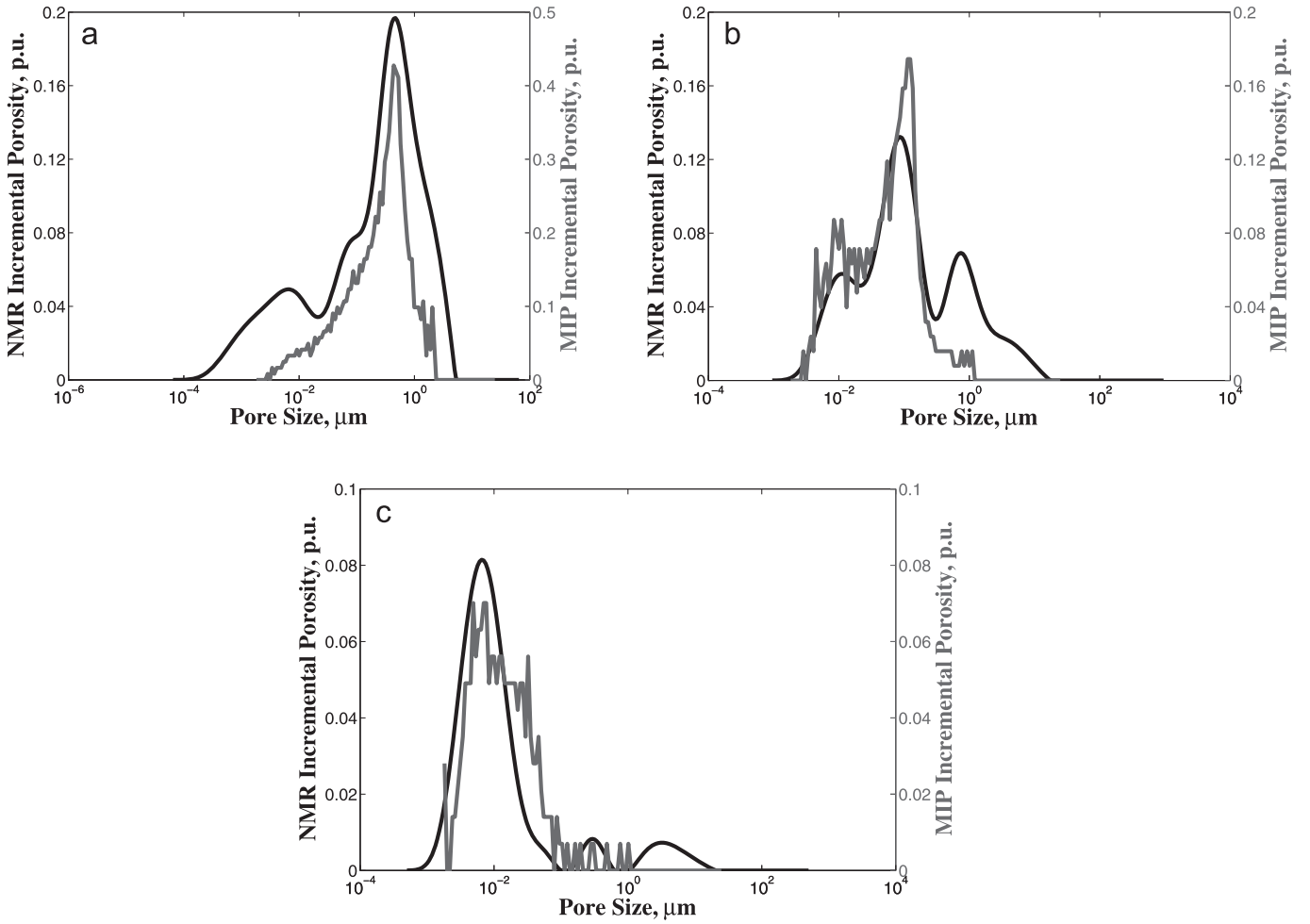

Fig. 14. Comparison of PSD (NMR) and TSD (MICP) for reservoir sandstone (a), non-reservoir sandstone (b) and siltstone (c), respectively. T_2 is converted into pore radius values the method described by Marschall et al. (1995). There is a good match between throat size and pore size. Similar behavior of throat size and pore size validates rock typing using NMR and MICP. Information about NMR PSD classification can be applied to downhole measurements and different rock types can be identified from NMR logs.

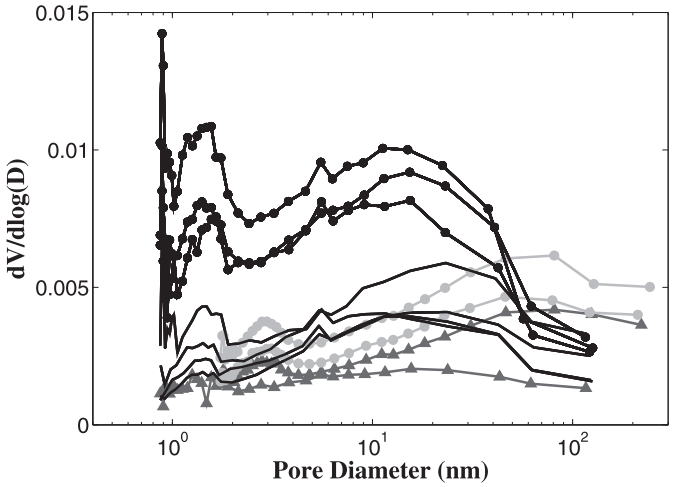

Fig. 15. Rock classification using nitrogen adsorption data. Area under curve graphically represents pore volume. Mudstone samples (black circles) show the highest pore volume. Siltstone (black colored curves) and reservoir sandstone (dark grey triangles) and non-reservoir sandstone (light grey circles) have subsequently lower readings. Different pore volumes are related to the amount of pores associated with clay.

other hand, the presence of relatively bigger pores in reservoir sandstone group is associated with the longer relaxation times. Effect of cementation on pore and throat sizes in non-reservoir sandstone led to the wide range of T_2 without demonstrating a dominant peak. The logarithmic mean of T_2 (T_{2LM}) for each group represents the dominant pore size for NMR log interpretation purposes. For reservoir, non-reservoir sandstones and siltstone T_{2LM} values are 22.2 ms, 3.4 ms and 0.29 ms, respectively. Note that NMR measurements were not performed on mudstone samples due to very fast relaxation. However, for mudstone T_{2LM} is expected to be in the range or smaller than siltstone due to abundance of clay minerals and small pores.

To qualitatively compare PSD from NMR to TSD from MICP, T_2 is converted into pore radius values using the method described by Marschall et al. (1995) (Fig. 14). Similar behavior of throat size and pore size validates rock typing using NMR and MICP. Information about NMR PSD classification can be applied to downhole measurements and different rock types can be identified from NMR logs.

In MICP and NMR rock typing, siltstone and mudstone are treated as one rock group. However, nitrogen adsorption (N_2) data in Fig. 15 show a distinction between siltstones and mudstones. Area under the curve graphically represents pore volume. Mudstone samples (black circles in Fig. 15) show the highest pore volume. Siltstone (black colored curves in Fig. 15), reservoir

Please cite this article in press as: Aliyev, E., et al., Rock typing of tight gas sands: A case study in Lance and Mesaverde formations from Jonah field, Journal of Natural Gas Science and Engineering (2016), http://dx.doi.org/10.1016/j.jngse.2015.12.045

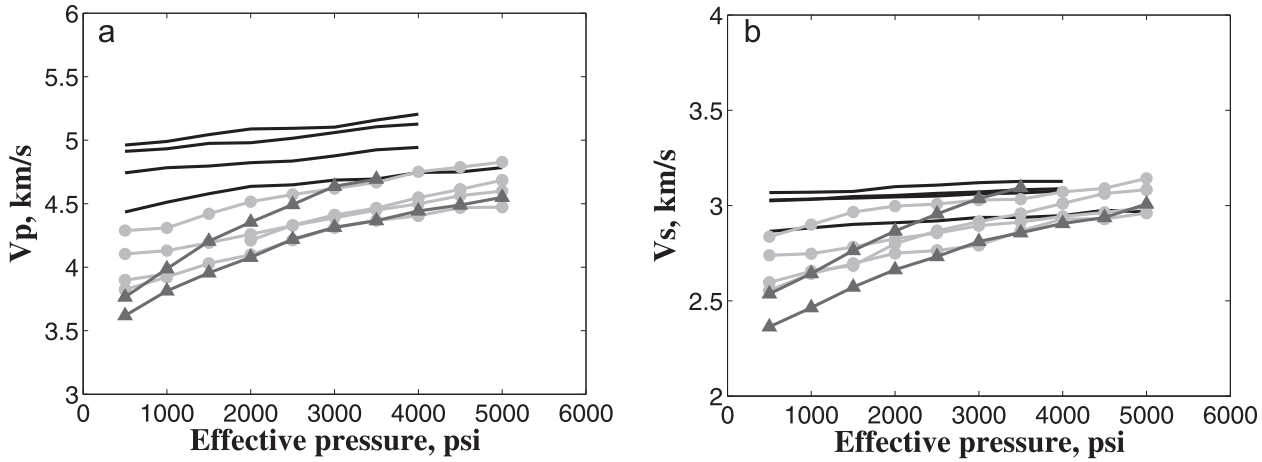

Fig. 16. Compressional (a) and shear (b) velocity under confining pressure conditions. Experiments were performed with zero pore pressure. Color codes show different rock types: reservoir sandstone (dark grey triangles), non-reservoir sandstone (light grey circles) and siltstone (black colored curves). Pressure cycle for this experiment is 0–5000 psi.

sandstone (dark grey triangles in Fig. 15) and non-reservoir sandstone (light grey circles in Fig. 15) have subsequently lower readings. Different pore volumes are mainly related to the pores associated with clay minerals. Mudstones have higher clay content than siltstone, hence the PSD measured by nitrogen adsorption shows higher amplitudes for mudstones. Lowest clay content belongs to reservoir sandstone samples (dark grey triangles in Fig. 15). Dominant pore size for this sample is 400 nm, which is larger than nitrogen adsorption limit (200 nm). Therefore, nitrogen method is incapable of capturing entire spectra of the pore size distribution in these samples. Pore volume and dominant pore size extracted from nitrogen adsorption method are not reliable for sandstones. Using nitrogen adsorption data, we identified fourth rock type which is mudstone. This group could not be differentiated from siltstone by MICP or NMR methods due to the limitations of each technique. Identifying the Mudstones can be applied in water saturation calculation using dual water model. The density and neutron porosity log values for Mudstone are not reliable due to borehole enlargement effects. Therefore, having true porosity of mudstone rock group from N_2 data increases the accuracy of water saturation calculation.

5.3. Ultrasonic velocity

Variation of aspect ratio controls pressure dependency of ultrasonic velocities. Greenfield and Graham (1996) relate pressure dependency of velocities to the presence of low aspect ratio cracks. Pores with low aspect ratio values tend to close under low confining pressures. As cracks close, velocity increases exponentially. Exponential growth is followed by linear buildup of velocity at crack closure pressure. Compressibility of formations are related to exponential part of the pressure dependency of velocities. In linear part of the behavior, velocity depends on matrix properties rather than cracks. Therefore, compressibility does not demonstrate visible change under high pressure loading. Fig. 16 (a) and (b) show compressional and shear velocities for different type of rocks; reservoir sandstone (dark grey triangles), non-reservoir sandstone (light grey circles) and siltstone (black colored curves). Pressure cycle for this experiment is 0–5000 psi, which is in the range of exponential velocity growth. This pressure cycle is equivalent to the effective stress during production from Mesaverde formation, Jonah field. Compressibility shows noticeable change and experiment mimics reservoir condition. To emphasize the effect of

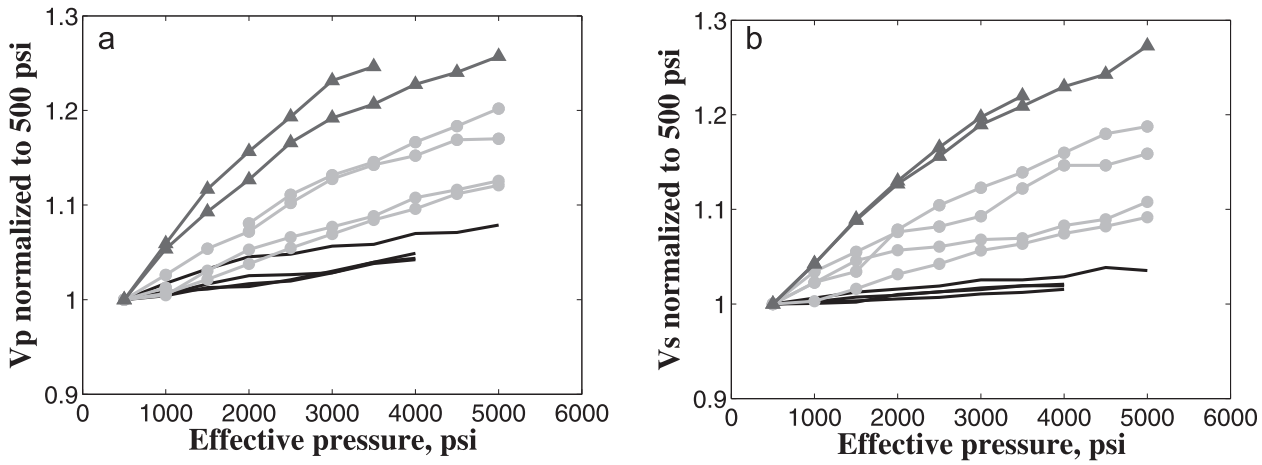

Fig. 17. Normalized compressional (a) and shear (b) velocities. Color codes show different rock types: reservoir sandstone (dark grey triangles), non-reservoir sandstone (light grey circles) and siltstone (black colored curves). Clear separation of reservoir sandstone, non-reservoir sandstone and siltstone is seen based on compressibility behavior during initial pressure loading. Reservoir sandstone demonstrates highest compressibility.

Please cite this article in press as: Aliyev, E., et al., Rock typing of tight gas sands: A case study in Lance and Mesaverde formations from Jonah field, Journal of Natural Gas Science and Engineering (2016), http://dx.doi.org/10.1016/j.jngse.2015.12.045

Table 1
Advantages and disadvantages of different rock typing techniques.

	Advantages	Disadvantages
Flow zone indicator (FZI)	- Quantitative evaluation of permeability and porosity for different rock types - Works better for high porosity and permeability	- Difficult to measure pore geometry in the lab - Uncertainty in low porosity and permeability;
Effective specific surface (ESS)	- Quantitative evaluation of permeability and porosity for different rock types - Works better for high porosity and permeability	- Difficult to measure specific surface area in the lab - Uncertainty in low porosity and permeability
Hydraulic rock typing (HRT)	- Quantitative evaluation of permeability and porosity for different rock types; - Works better for high porosity and permeability	- Requires mercury injection data; - Reliability of permeability and porosity data in tight formations due to tool limitations;
TSDs from mercury injection Capillary pressure (MICP)	- Quantitative evaluation of effective porosity for different rock types - Detection of cementation effects; - Reliable in tight formations	- Unable to detect pore throat with diameter less than 3.6 nm;
PSDs from nuclear magnetic resonance (NMR)	- Application to downhole logging (NMR); - Applicable to entire range of porosity and permeability;	- Poor resolution in clay-rich formations
PSDs from BET nitrogen adsorption	- Evaluation of porosity for clay rich formations; - Application to downhole logging (GR, density)	- Applicable to the pore size range of 1.7–193.5 nm
Pressure dependency of ultrasonic velocities	- Qualitative evaluation of pore compressibility	- Sensible to natural and post drilling induced fractures

compressibility behavior, velocity data is normalized to the pressure value at 500 psi (Fig. 17). Clear separation of reservoir sandstone, non-reservoir sandstone and siltstone is seen based on compressibility behavior during initial pressure loading. Reservoir sandstone demonstrates highest compressibility.

6. Conclusions

In this study, we investigated three available rock typing techniques: FZI, ESS and HRT. HRT method showed improved porosity and permeability correlation by considering the dominant pore size from MICP data. We also classified the samples using MICP, NMR and nitrogen adsorption data in Lance and Mesaverde formations from Jonah field. Based on pore size distribution, four distinct rock types are identified: reservoir sandstone, non-reservoir sandstone, siltstone and mudstone. The advantages and disadvantages of different rock typing methods are summarized in Table 1. Combination of gamma ray, porosity and NMR logs can be used to apply this rock typing study at downhole condition. The main conclusions of this study are summarized as:

- Comparison of hydraulic rock typing (HRT), flow zone indicator (FZI) and ESS area demonstrates that HRT method is more reliable in classification of sandstones by flow properties for Mesaverde and Lance Formations.
- MICP pore throat distribution shows that dominant pore throat size for reservoir and non-reservoir sandstones are 400 and 100 nm, respectively. Pore size from NMR demonstrated equivalent behavior to pore throat size from MICP. The logarithmic mean values of T_2 transverse relaxation times for reservoir, non-reservoir sandstone and siltstone/mudstone are 22.2 ms, 3.4 ms and 0.29 ms, respectively.
- Fourth rock group – mudstone was not detected by MICP or NMR methods. Mudstones were separated from siltstones based on log differential pore volume distribution from N_2 adsorption data.
- Ultrasonic velocities demonstrate pressure dependency during initial loading. Based on compressibility behavior three rock types were confirmed: reservoir sandstone, non-reservoir sandstone and siltstone. Reservoir sandstone has highest compressibility.

Acknowledgments

This paper is dedicated to the memory of Dr. Michael L. Batzle. We are thankful to Azar Hasanov, Kurt Livo, Cesar Mapeli and Yijia Zhang from Colorado School of Mines for performing some parts of the measurements. We acknowledge OCLASSH and Fluids consortiums at Colorado School of Mines for funding of the project. We also acknowledge Exaro Energy III LLC for providing core samples and data.

References

Alam, M.M., Fabricius, I.L., Prasad, M., 2011. Permeability prediction in chalks. AAPG Bull. 95 (11), 1991–2014.
Amaefule, J.O., Altunbay, M., Tiab, D., Kersey, D.G., Keelan, D.K., 1993. Enhanced reservoir description: using core and log data to identify hydraulic (ow) units and predict permeability in uncored intervals/wells. In: SPE Annual Technical Conference and Exhibition. Society of Petroleum Engineers.
Archie, G.E., 1950. Introduction to petrophysics of reservoir rocks. AAPG Bull. 34 (5), 943–961.
Barrett, E.P., Joyner, L.G., Halenda, P.P., 1951. The determination of pore volume and area distributions in porous substances. i. computations from nitrogen isotherms. J. Am. Chem. Soc. 73 (1), 373–380.
Butler, J., Reeds, J., Dawson, S., 1981. Estimating solutions of first kind integral equations with nonnegative constraints and optimal smoothing. SIAM J. Numer. Anal. 18 (3), 381–397.
Carr, H.Y., Purcell, E.M., 1954. Effects of diffusion on free precession in nuclear magnetic resonance experiments. Phys. Rev. 94 (3), 630.
Castillo, P., Ou, L., Prasad, M., 2012. Petrophysical description of tight gas sands. In: 2012 SEG Annual Meeting. Society of Exploration Geophysicists.
Cluff, S.G., Cluff, R.M., 2004. Petrophysics of the Lance sandstone reservoirs in Jonah field, Sublette County, Wyoming. AAPG Stud. Geol. 52, 215–241.
Comisky, J.T., Santiago, M., McCollom, B., Buddhala, A., Newsham, K.E., 2011. Sample size effects on the application of mercury injection capillary pressure for determining the storage capacity of tight gas and oil shales. In: Canadian Unconventional Resources Conference. Society of Petroleum Engineers.
DuBois, D., Wynne, P., Smagala, T., Johnson, J., Engler, K., McBride, B., 2004. Geology of Jonah Field, Sublette County, Wyoming.
Dunn, K.-J., LaTorraca, G., Warner, J., Bergman, D., 1994. On the calculation and interpretation of NMR relaxation time distributions. In: 69th Annual SPE Technical Conference and Exhibition. SPE Paper, 28369.
Greenfield, R.J., Graham, E.K., 1996. Application of a simple relation for describing wave velocity as a function of pressure in rocks containing microcracks. J. Geophys. Res. Solid Earth (1978-2012) 101 (B3), 5643–5652.
Hanson, W., Vega, V., Cox, D., 2004. Structural geology, seismic imaging, and genesis of the giant Jonah gas field, Wyoming, USA. In: Jonah Field: Case Study of a Giant Tight-Gas Fluvial Reservoir: Rocky Mountain Association of Geologists, Volume 52 of AAPG Studies in Geology, pp. 61–92.
Harkins, W.D., Jura, G., 1944. Surfaces of solids. xii. An absolute method for the determination of the area of a finely divided crystalline solid. J. Am. Chem. Soc. 66 (8), 1362–1366.
Marschall, D., Gardner, J., Mardon, D., Coates, G., 1995. Method for correlating NMR

Please cite this article in press as: Aliyev, E., et al., Rock typing of tight gas sands: A case study in Lance and Mesaverde formations from Jonah field, Journal of Natural Gas Science and Engineering (2016), http://dx.doi.org/10.1016/j.jngse.2015.12.045

relaxometry and mercury injection data. In: 1995 SCA Conference, Paper, Number 9511.
Meiboom, S., Gill, D., 1958. Modified spin-echo method for measuring nuclear relaxation times. Rev. Sci. Instrum. 29 (8), 688–691.
Mortensen, J., Engstrom, F., Lind, I., 1998. The relation among porosity, permeability, and specific surface of chalk from the Gorm field, Danish North Sea. SPE Reserv. Eval. Eng. 1, 245–251.
Pittman, E.D., 1992. Relationship of porosity and permeability to various parameters derived from mercury injection-capillary pressure curves for sandstone (1). AAPG Bull. 76 (2), 191–198.
Prasad, M., 2003. Velocity-permeability relations within hydraulic units. Geophysics 68 (1), 108–117.
Rose, W., Bruce, W., 1949. Evaluation of capillary character in petroleum reservoir rock. J. Pet. Technol. 1 (05), 127–142.
Rushing, J.A., Newsham, K.E., Blasingame, T.A., 2008. Rock typing: keys to understanding productivity in tight gas sands. In: SPE Unconventional Reservoirs Conference. Society of Petroleum Engineers.
Saidian, M., Kuila, U., Rivera, S., Godinez, L.J., Prasad, M., 2014, August 28. Porosity and pore size distribution in mudrocks: a comparative study for Haynesville, Niobrara, Monterey and Eastern European Silurian formations. Society of Petroleum Engineers. http://dx.doi.org/10.15530/urtec-2014-1922745.
Thomeer, J., 1960. Introduction of a pore geometrical factor defined by the capillary pressure curve. J. Pet. Technol. 73–77.
Vernik, L., Kachanov, M., 2010. Modeling elastic properties of siliciclastic rocks. Geophysics 75 (6), E171–E182.
Washburn, E.W., 1921. Note on a method of determining the distribution of pore sizes in a porous material. Proc. Natl. Acad. Sci. U. S. A. 115–116.

Please cite this article in press as: Aliyev, E., et al., Rock typing of tight gas sands: A case study in Lance and Mesaverde formations from Jonah field, Journal of Natural Gas Science and Engineering (2016), http://dx.doi.org/10.1016/j.jngse.2015.12.045